Surface Soil Moisture Estimation in Bare Ground and Vegetated Areas Using a Neural Network Model

Tarakanta Maharana, Nalanda Institute of Technology, Bhubaneswar
E-mail-tarakanta@thenalanda.com

Abstract- The majority of methods for measuring surface soil moisture (SSM) using optical and thermal infrared (TIR) spectroscopies are designed to compute several characteristic bands or indices and then create a regression connection between them using measurement data. Yet, the regression relationship frequently exhibits nonlinearity as a result of the combined influence of several factors. However, it is challenging to develop a more comprehensive model for the remote sensing (RS) estimate of SSM because the link between the single temporal picture and the measured data is not transplantable in time and space. The back propagation (BP) neural network (NN) is used to identify the link between the characteristic band/index and the measurement data. This network has good nonlinear mapping capabilities.

1. Introduction

Soil water content (SWC) is a crucial variable in meteorology, hydrology, and agricultural science that significantly affects water displacement, vegetation photosynthesis, and land surface evaporation [1, 2]. The groundwater, surface water, and atmospheric water cycle systems are connected by it [3, 4]. Soil moisture (SM) monitoring accuracy is crucial for the correct prediction of climate change [5, 6]. Although direct measurement is the most precise way to track SM, in situ measurement data are ineffective in displaying the geographical distribution of SM and cannot be used to track large-scale changes in SM's spatial and temporal characteristics [7, 8].

The development of a remote sensing (RS) data algorithm provides an efective solution to the large-scale monitoring of surface soil moisture (SSM) [9, 10].

Various RS methods have been developed in diferent regions of the electromagnetic spectrum. These methods may be classified into three major groups: microwave (MW), thermal infrared (TIR), and optical [11, 12]. Microwave is advantageous due to its stronger penetration ability, longer wavelength, and the robustness to adverse weather conditions. Therefore, MW technology shows a greater potential in monitoring global SM dynamics [13]. However, due to the relatively rough resolution of SM products provided by Soil Moisture Active Passive (SMAP) mission and Soil Moisture and Ocean Salinity (SMOS) mission, they are not suitable for small-scale regional applications. Apart from that, a challenge presented by using MW to monitor SSM is the need to input various physical parameters, some of which are still not well defined at present [14]. For example, surface roughness, which is easily changeable, must be measured in the field, which is time-consuming.

Compared with MW SM products, optical/TIR RS data usually have a higher spatial resolution, which can well meet the needs of SM data in various fields [15]. Optical methods apply the visible, near infrared (NIR), and shortwave infrared (SWIR) data for SM retrieval. Many scholars have used diferent vegetation indices to monitor SM and dryness [16]. However, there is a certain lag in vegetation growth for the degree of surface drought. Some other studies used spectral feature space to construct SSM retrieval models. For example, the perpendicular drought index (PDI) [17] is derived from the red and near infrared (NIR) band reflectance triangular space. This method needs to determine the soil line artificially to realize the model. However, the distribution of soil lines highly depends on some parameters, such as soil minerals, iron oxide content, particle size distribution, and organic matter [18]. Although TIR methods are developed based on physical principles, the methods are usually empirical and depend on local meteorological conditions, such as humidity, temperature, and wind speed, and thus, the measurement results vary temporally and with land cover types [19, 20].

The combination of optical and TIR RS data mostly results in better accuracy for SM retrieval. To some extent, land surface temperature (LST) can be taken as an indicator of the change in SM and vegetation. Therefore, the retrieval model based on LSTand vegetation index (VI) can be used to estimate SM [21]. The temperature vegetation dryness index (TVDI) is parameterized based on the LST-VI space [22]. Over the past two decades, this simple model and those improved models in relation to it have already been applied to SSM estimation [23–26]. Despite this, the spatial distribution of LST-VI remains possible not to conform to triangle or trapezoid, thus afecting the accuracy of SM estimation. The spatial shape is treated as a triangle or trapezoid in the context of human intervention, which can lead to uncertainty in the calculation results.

A major method of estimating SWC based on optical and thermal infrared data is to retrieve the SM index or drought index using satellite data [27–30], so as to establish the regression relationship between the index and the actual SWC using the measurement data [31]. However, the variation of SWC can be afected by various factors (e.g., soil texture, surface roughness, topography, temperature, and vegetation coverage), which leads to the nonlinear regression relationship. Moreover, the relationship between the single temporal image and the measurement data is not transferable in time and space, which makes it challenging to establish a more general model of RS estimation for SM.

Compared with those traditional methods, the neural network (NN) model demonstrates various advantages, including the flexibility in combining information from diferent sources and mapping the input-output relationship of any data without needing an empirical formula [32]. The statistical relationship between satellite observation and SSM can be simulated on the basis of satellite data and measured SM estimation without explicitly establishing any physical connection. The excellent nonlinear mapping ability of the NN model makes it capable to minimize uncertainty and improve the accuracy of SM retrieval from RS data [33–35].

Some scholars have constructed an NN model based on microwave data for estimating soil moisture [36, 37]. There is also a synergistic use of microwave and optical data to retrieve soil moisture using NN models [38, 39]. In these studies, NN models estimated soil moisture with a high degree of accuracy. Some studies have used the normalized diference vegetation index calculated by optical data and land surface temperature calculated from thermal infrared data as parameters into the neural network model to estimate soil moisture [40]. Optical and thermal infrared data have an exceptional potential for estimating soil moisture. However, there are few studies on SM estimation using optical and TIR data with the NN model.

The primary purpose of this paper is to build a highly universal SM retrieval model, which can overcome the influence of soil texture, vegetation cover, terrain, and other factors. As one variety of the ANN, the back propagation (BP) neural network (NN) is applied to construct the SM prediction model. The characteristic band/index with high resolution and multitemporal data is taken as the input data, while the measured SM is treated as the output data. Finally, the multiple spatial and temporal Landsat-8 and MODIS data were used to estimate SSM. The model constructed in this paper is universal and can be applied to estimate SM in both bare land and vegetated areas.

2. Study Area and Data Source

Study Area. As shown in Figure 1, the study area is located in the middle of the Tibetan Plateau. The map of China is downloaded from website https://bzdt.ch.mnr.gov. cn/index.html. The climate in the Naqu area is relatively warm from May to September each year, and this period refers to the season of vigorous vegetation growth. During this period, the land cover is dominated by plateau meadow. The other period includes the snow and soil freezing period, during which most areas are covered by snow and frozen soil. As impacted by low biomass, air quality, and humidity,the MW signal attenuation is weak, so this area acts as an ideal place to verify satellite and model simulation of SM products [41].

In Situ Measurements. The measured SM data used in this study originated from the SM observation network in the Naqu area. There were 57 stations available in the network, with SM and temperature data at four observation depths (i.e., 5, 10, 20, and 40 cm), and the sampling interval was 30 min. The mentioned measurements provided con- siderable valuable experimental data for SM retrieval in the Tibetan Plateau [42]. In the present study, the measured SMdata from 2014 to 2016 were collected to assess the per- formance of the SSM retrieval model. The dataset is provided by the National Tibetan Plateau Data Center.

Remote Sensing Data. Landsat 8 carries Operational Land Imager (OLI) and Thermal Infrared Sensor (TIRS). The OLI provides nine optical bands, and the TIRS provides twothermal bands. Twelve Landsat-8 images

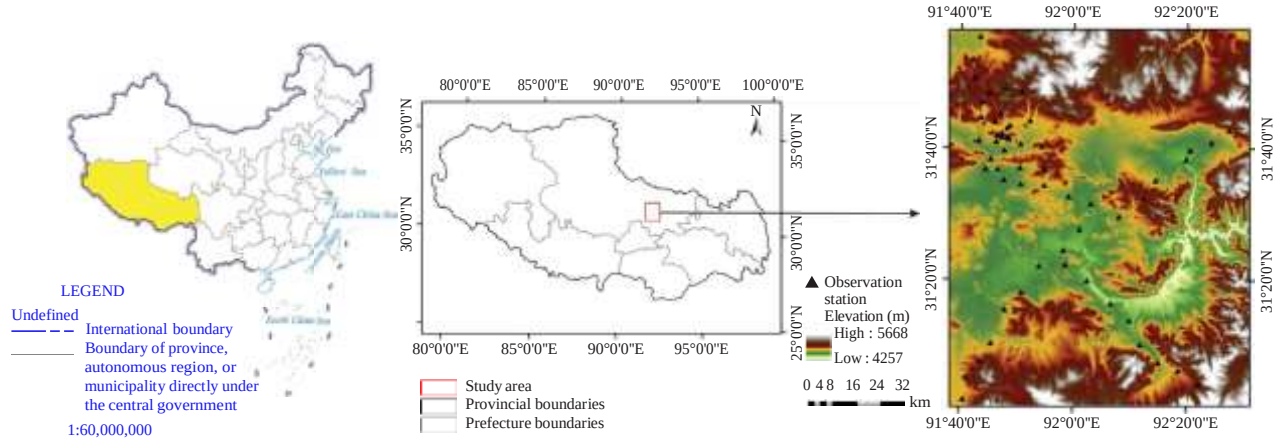

Figure 1: Location of the study area.

May, 18 June, and 27 July, 2014; 20 May, 23 July, 30 July, 31 August, 9 September, and 16 September, 2015; 25 July and 17 August, 2016, were acquired.

3. Research Method

By using the BPNN, the coastal, blue, green, red, NIR, shortwave infrared (SWIR) band, and LST were taken as the input data, the measured soil volumetric moisture was taken as the output data, and the SM retrieval model is established. The LST data were calculated using the TIRS1 and TIRS2 bands of Landsat-8. In addition, the observed SM data are used to test the results of model estimation and evaluate retrieval accuracy.

BPNN Model. The BPNN refers to a type of the mul- tilayer feed-forward network with a hidden layer. In the practical application of ANNs, the BP network has been extensively used in data compression, pattern recognition, aswell as function approximation. The BP network consists of an input layer, hidden layer, and output layer. The BPNN comprises an input layer, a hidden layer, and an output layer. The structure with a single hidden layer of the BPNN is shown in Figure 2. All neurons were configured according to the model shown in Figure 3.

The training operation of the BPNN consists of signal forward propagation and error back propagation. Forward propagation means that the input signal was transmitted from the input layer via the hidden layer to the output layer. If the output layer yields the desired output (the actual output is consistent with the expected output), the learning algorithm ends; otherwise, it turns to back propagation. Back propagation aims to reduce the error by calculating the error according to the original connection path direction and adjusting the weight and threshold of each layer node based on the gradient descent method. After repeated learning and training, the network parameters (weight and threshold) are determined for the minimum error and the training is terminated. At this point, the trained NN is capable to process the input information of similar samples and to output the nonlinear converted information with the minimum error.

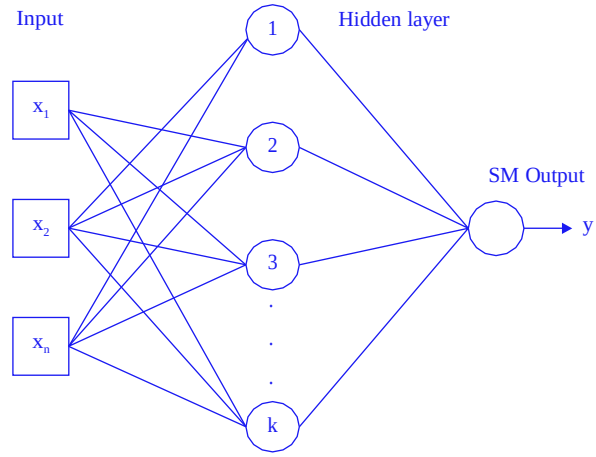

Figure 2: Topological structure diagram of the BPNN.

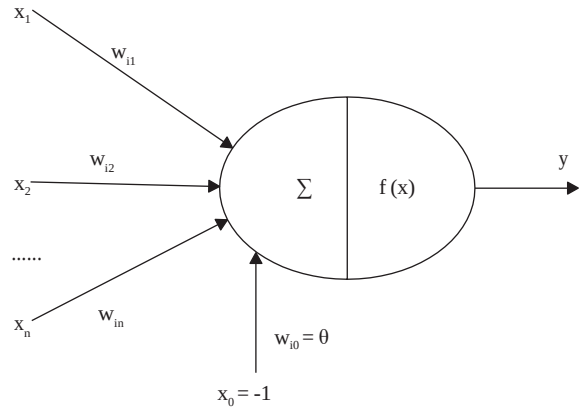

Figure 3: Single neuron structure.

Input Parameter Scheme. The approach to monitoring SM with optical data is mainly based on the spatial shape of pixel distribution in Landsat-8 bands to estimate SM. The SWIR 1 and SWIR 2 bands of Landsat-8 data (1650 nm corresponding to band 6, 2210 nm corresponding to band 7)are sensitive to SWC, especially at 2210 nm [43]. In this

Table 1: Parameter setting of diferent schemes.

Scheme	Input variables	Output variable
1	Coastal, blue, green, red, NIR, SWIR	Measured soil volume water content
2	Blue, green, red, NIR, SWIR	
3	Red, NIR, SWIR	
4	Red, NIR	
5	NIR, SWIR	
6	Red, SWIR	
7	Coastal, blue, green, red, NIR, SWIR, LST	
8	Blue, green, red, NIR, SWIR, LST	
9	Red, NIR, SWIR, LST	
10	Red, NIR, LST	
11	NIR, SWIR, LST	
12	Red, SWIR, LST	

study, the SWIR 2 is taken as the input parameters of the SSM estimation model.

There are twelve schemes that were constructed to analyze the efect of various parameters on the accuracy of SSM estimation (Table 1). Scheme 1 sets all optical bands as input parameters. Based on the formula expressing SM in Tasselled Cap transformation, the band used in the formula was taken as the input parameter of scheme 2. According to the previous models applied to calculate SM through optical data, it can be found out that there were only a small number of bands in red, NIR, and SWIR bands as used in these models, so that schemes 3–6 were designed. On the basis of schemes 1–6, the LST data were introduced, respectively, with schemes 7–12 set.

4. Results

SSM Estimation Results and Validation. In the experi- ment, a total of 252 sample data were extracted from the study area. In addition, the BPNN was set below: the training sample was 189 and the test sample was 63. In order to ensure the stability of the BPNN model, we trained the BPNN model100 times to obtain the correlation coefficient of estimating and measuring soil moisture. Finally, the average value of 100 training results is selected as the estimation accuracy of the model. The in situ measured soil volumetric moisture was used as a reference to calculate the coefficient , root mean square error (RMSE), unbiased root mean square error (ubRMSE), and bias (Bias) of the estimated SSM. Figure 4 shows the scatter distribution of soil volumetric moisture estimated and measured by 12 schemes. Table 2 shows the accuracy of the estimated SSM in each scheme.

With only the optical bands as the input parameters of the SM estimation model (schemes 1–6), the estimated SM shows correlation with the measured value to a certain extent, and the correlation coefficient reaches up to 0.8682, which renders the accuracy of retrieval poor. In the scheme of estimating SM with optical data, all bands were treated as input to obtain the most accurate SM (scheme 1). In scheme 2, the r between the estimated and measured SM is 0.8163. After removing the coastal band, the estimation accuracy of SM does not change significantly. As for the input, only the red, NIR, and SWIR bands are retained (scheme 3). Whereas, the estimation accuracy of SM remains comparable to that of scheme 1, indicating that the red, NIR, and SWIR bands play a major role in SM estimation.

In schemes 7–12, the input parameters were set as optical bands and LST, and the estimated SSM was closer to the observation. The SM estimated by scheme 7 had the highest accuracy. It showed a RMSE of 0.0017 and r of 0.9001. The normalized diference vegetation index (NDVI) and normalized diference water index (NDWI) were calculated by red, NIR, and SWIR bands. According to the LST-VI SM estimation model, schemes 10–11 of red, NIR, SWIR, and LST are designed as input parameters. Scheme 11 shows a higher estimation accuracy of SSM than that of scheme 10, which suggests that NDWI is more suitable to represent VI for SSM estimation than NDVI. With red, SWIR band, and LST as input parameters (scheme 12), the SM estimation accuracy was higher than in schemes 10 and 11.

When using the BPNN model to retrieve soil moisture, the soil moisture with the highest accuracy can be estimated by selecting scheme 7. In case of lack of TIR data, scheme 1 is preferred to retrieve soil moisture.

Land Surface Feature Influence on SSM Estimation Results. Zhang et al. [44] used the random forest model, which had land surface feature parameters and in situ soil moisture data to predict SSM. It would be good to test the same experiment on a diferent environment to check the consistency of the results. To analyse the influence of land surface feature factors on SSM estimation results, the ele- vation, slope, aspect, and vegetation coverage (normalized diference vegetation index, NDVI) factors were added into BPNN model. The soil texture of all observation stations in the study area is the same type, so this factor was not considered. On the basis of scheme 7, each influence factor was added, respectively. The estimated soil moisture were grouped according to the value of the influence factors. Also, the r between each group of data and the corresponding measured soil moisture were discussed (Table 3).

With the increase of elevation and slope, the r between estimated and measured SSM gradually decreases. The r of the north aspect was obviously lower than that of other aspects. The terrain of Naqu study area fluctuates violently, and it was easy to have shadow in areas with large elevation, steep slope, and north aspect. In the shadow areas, the

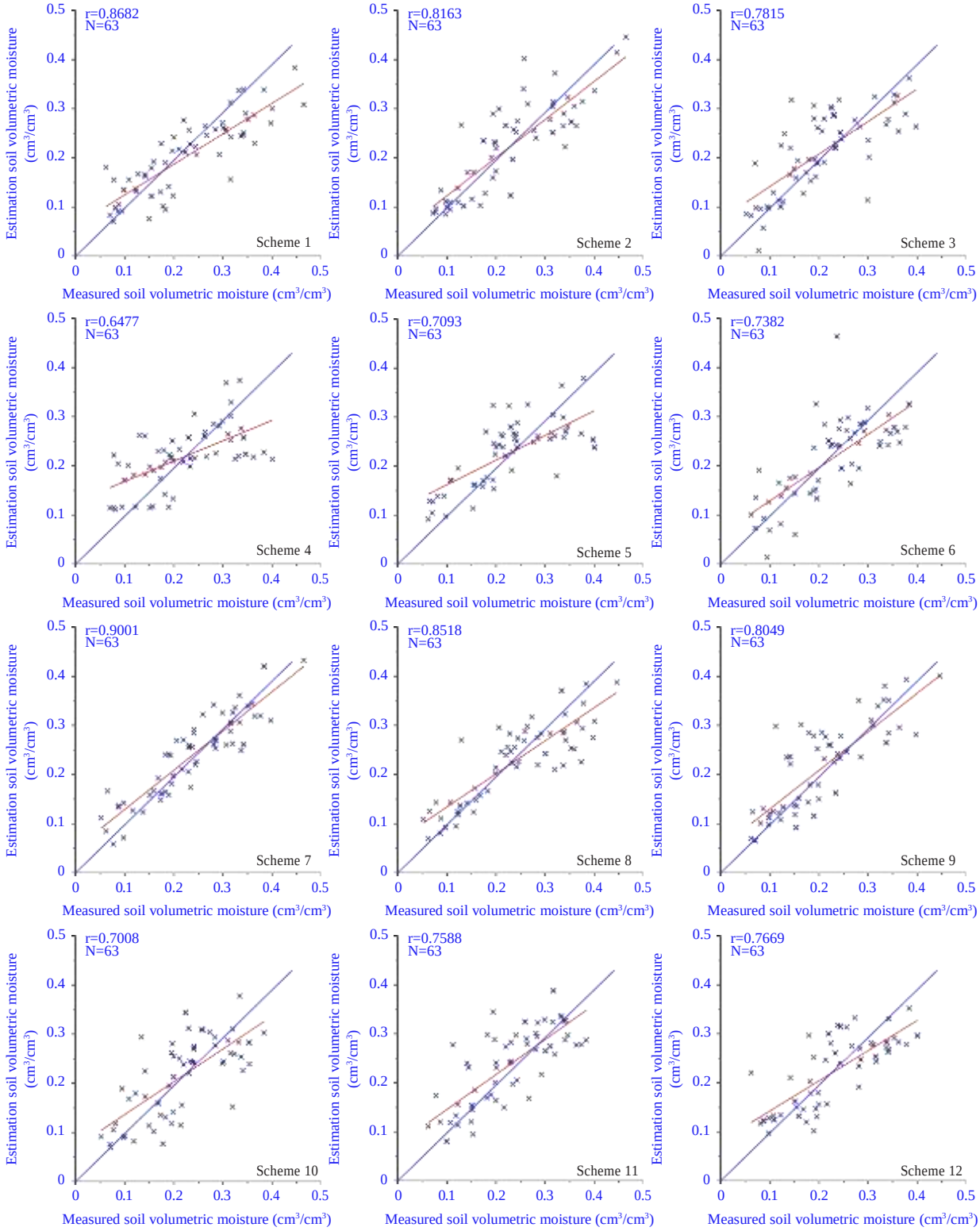

Figure 4: The scatter plot between measured and estimated soil volumetric moisture. A 1 : 1 line was added to the map.

surface reflectance is very low, and the satellite data in this area will greatly reduce the accuracy of estimated SSM. It is worth noting that the mountain shadow in the southern hemisphere appears on the south aspect. In areas with diferent NDVI values, the *r* values of estimated and measured SSM were similar. Vegetation coverage will not significantly afect SSM estimated by the BPNN model.

BPNN is not afected by the underlying surface condition and can be applied to areas with diferent vegetation coverage. However, when using optical satellite data as input

Table 2: Accuracy evaluation of soil volumetric moisture retrieval results.

Evaluating indices	Scheme 1	Scheme 2	Scheme 3	Scheme 4	Scheme 5	Scheme 6	Scheme 7	Scheme 8	Scheme 9	Scheme 10	Scheme 11	Scheme 12
R	0.8682	0.8163	0.7815	0.6477	0.7093	0.7382	0.9001	0.8519	0.8049	0.7008	0.7588	0.7669
RMSE (cm^3/cm^3)	0.0593	0.0579	0.0577	0.0674	0.0648	0.0631	0.0414	0.0547	0.0579	0.0635	0.0575	0.0588
ubRMSE (cm^3/cm^3)	0.0544	0.0577	0.0575	0.0774	0.0646	0.0617	0.0414	0.0537	0.0574	0.0634	0.0569	0.0582
Bias (cm^3/cm^3)	−0.0035	−0.0034	−0.0033	−0.0045	−0.0042	−0.0039	−0.0017	−0.0030	−0.0033	−0.0041	−0.0033	−0.0034

Table 3: The results for BPNN in four groups respective to the pixels land surface feature values.

Elevation ≤ 4500 m	4500 m < Elevation ≤ 4600 m	4600 m < Elevation ≤ 4700 m	4700 m < Elevation
R	*r*	*r*	*r*
0.9197	0.9082	0.8552	0.8186
Slope ≤ 3.5°	3.5° < Slope ≤ 5.5°	5.5° < Slope ≤ 9°	9° < Slope
r	*r*	*r*	*r*
0.9283	0.8992	0.8138	0.7513
North aspect	East aspect	South aspect	West aspect
r	*r*	*r*	*r*
0.6972	0.8937	0.9395	0.8718
NDVI ≤ 0.25	0.25 < NDVI ≤ 0.40	0.40 < NDVI ≤ 0.55	0.55 < NDVI
R	*R*	*R*	*R*
0.8724	0.8801	0.8916	0.8786

parameters, the BPNN model is more suitable for the area with flat terrain and gentle slope. Also, BPNN cannot' construct the empirical formula to express the relationship between soil moisture and various parameters.

Application of the SSM Estimation Model. Since the grid size of Landsat data was 30 m × 30 m, the small-scale ob- servation network of the Naqu SM observation network wastaken as the retrieval area of SSM. Figure 5 shows the surface soil moisture map retrieved from scheme 7 on May 20, 2015. The soil volumetric moisture of the 9 stations estimated in the area ranged from 0.122 to 0.357 cm^3/cm^3 in accordance with the in situ data (0.145–0.395 cm^3/cm^3). The scatter plot between measured and estimated soil volumetric moisture isshown in Figure 5©. It showed a RMSE of 0.0429 and *r* of 0.8392. The result indicates that calibration of the BPNN model with in situ data generally leads to reasonable SM estimates.

5. Discussion

The PDI and TVDI models were used to retrieve soil moisture, respectively. The PDI and TVDI models were used to estimate SSM in the same area of Figure 5. The red and NIR bands shall be applied to calculate PDI (corresponding to scheme 4), while the red, NIR, and LST shall be applied to calculate TVDI (corresponding to scheme 10). The scatter plot of SM estimated and measured by PDI and TVDI is shown in Figure 6. The *r* between the estimated and mea- sured SM are 0.4786 and 0.5047, respectively. Comparing the SSM calculated by PDI and TVDI, the accuracy of SM calculated by the BPNN has significantly improved.

We also brought MODIS data into the BPNN model to estimate soil moisture. There is a slight diference between the band range of MODIS and Landsat-8 data (Table 4), and there is no coastal band in MODIS data. The LST data were obtained from MOD11A1 products. There are ten schemes (schemes 2–6 and schemes 7–12 in Table 1) to estimate SM using the BPNN.

We collected 742 MODIS data, 594 data were used as training samples, and the remaining 148 data were used as test samples. The retrieved SSM had the highest accuracy when the input parameters were green, blue, red, NIR, SWIR band, and LST data. The scatter plot between measured and estimated soil volumetric moisture is shown in Figure 7. It showed a RMSE of 0.0573 and *r* of 0.8164. The SSM esti- mation accuracy is similar to Landsat-8 data (scheme 8).

It is worth noting that the more the input sample data, the higher the accuracy of SSM retrieved by the BPNN. However, this method is not applicable in cloud and shadow-covered areas. Since the input parameters in the model are all derived from RS raster data, the images with diferent spatial resolutions can be used for the SSM esti- mation model based on the BPNN. Sentinel-2 is regarded as another ideal RS data due to its high temporal and spatial resolution.

The BPNN model is not limited by RS data. The RS images such as Landsat-8, MODIS, and Sentinel-2 can be used as input parameters to retrieve soil moisture. Since the BPNN model directly uses the surface spectral reflectance data to retrieve soil moisture, the model is not limited by regional conditions. The BPNN model can simultaneously retrieve soil moisture of bare soil and vegetated areas. However, when optical and TIR data are input into the NN

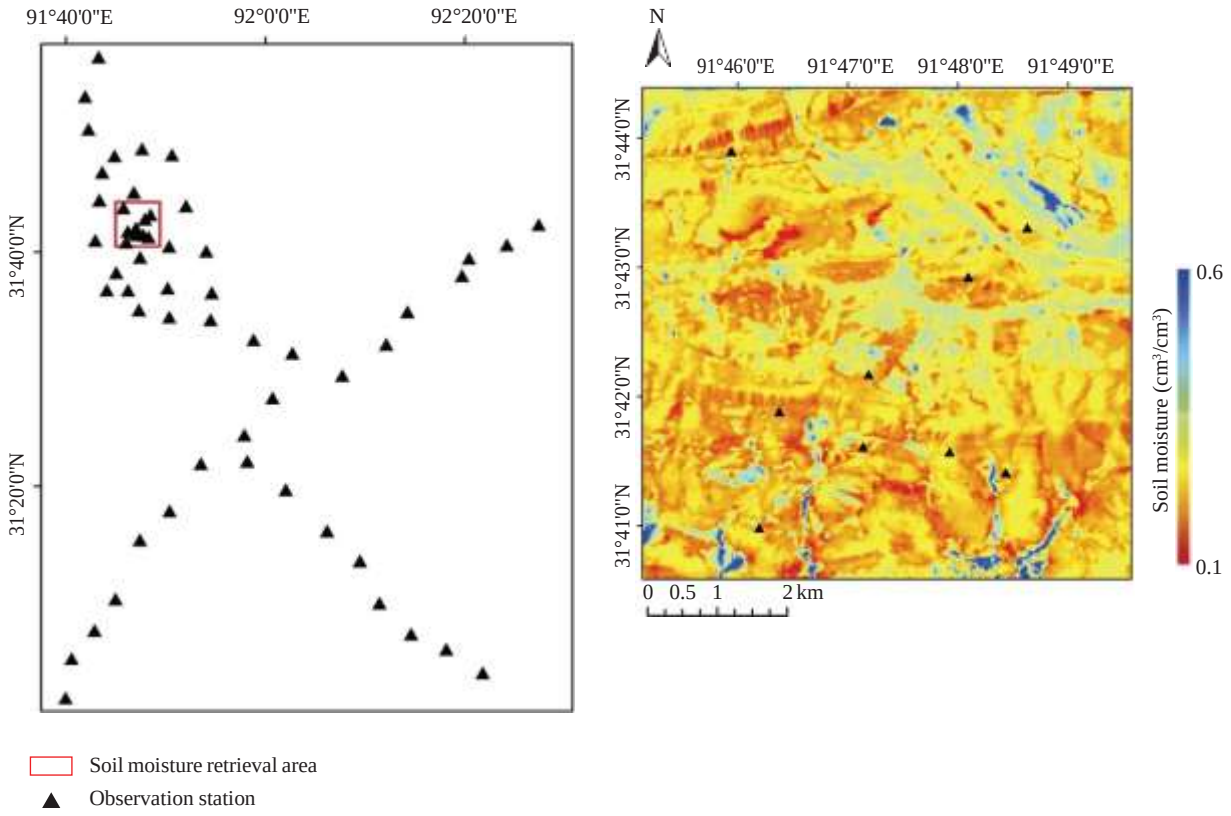

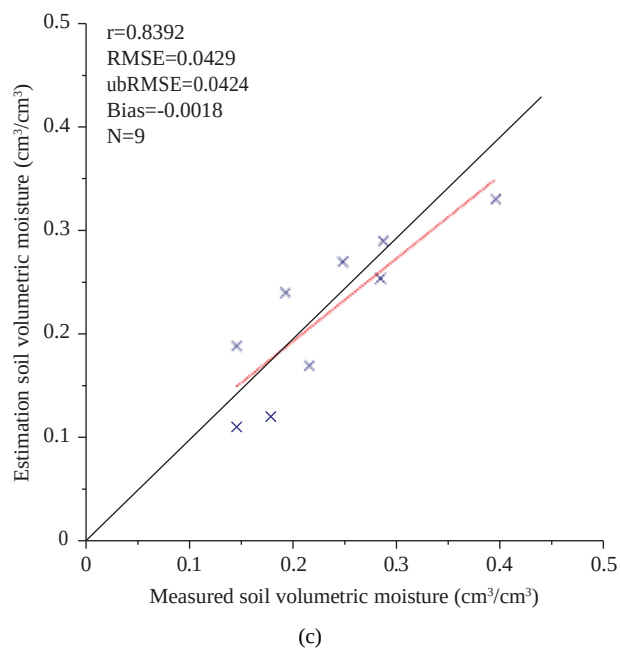

Figure 5: Soil moisture mapping in retrieval area on May 20, 2015.

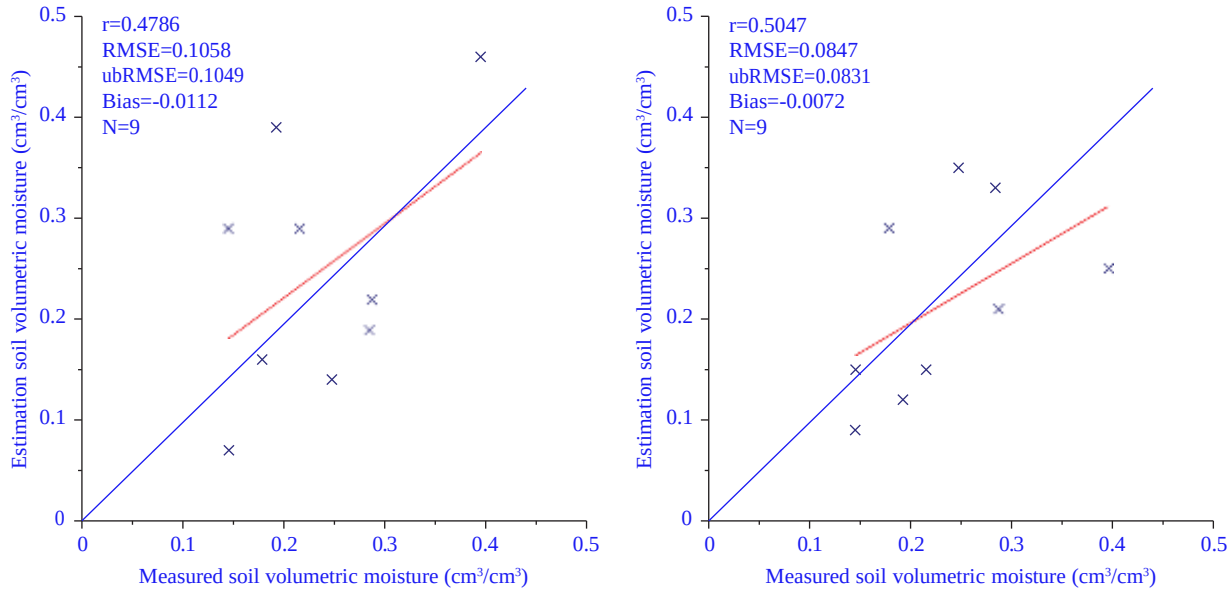

Figure 6: The scatter plot between measured and estimated soil volumetric moisture. A 1 : 1 line was added to the map. (a) PDI. (b) TVDI.

Table 4: Correspondence between MODIS and landsat-8 data bands.

MODIS	Wavelength range (nm)	Landsat-8	Wavelength range (nm)
Band 1	620–670	Band 4	630–680
Band 2	841–876	Band 5	845–885
Band 3	459–479	Band 2	450–515
Band 4	545–565	Band 3	525–600
Band 6	1628–1652	Band 6	1560–1660
Band 7	2105–2155	Band 7	2100–2300

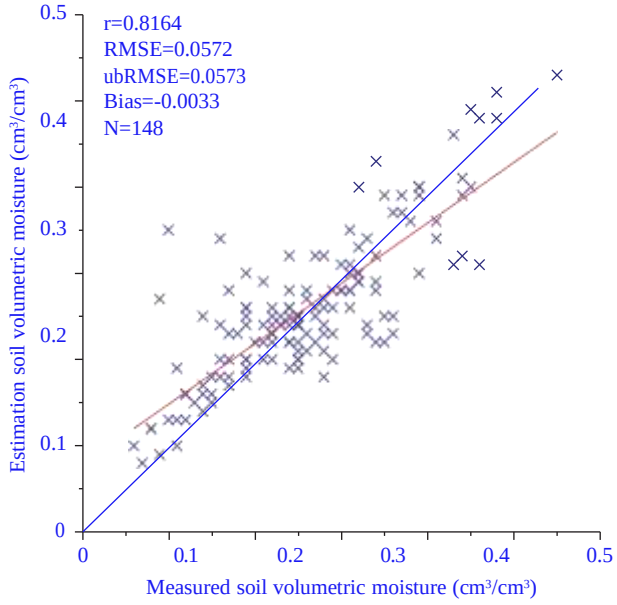

Figure 7: The scatter plot between measured and estimated soil volumetric moisture. A 1 : 1 line was added to the map.

model, it is necessary to exclude raster data that are obscured by clouds or afected by the atmosphere.

6. Conclusion

Combined with optical-thermal infrared RS data and measured soil volumetric moisture data, a retrieval model of SSM is established on the basis of the BPNN. It can be found that the BPNN is suitable for establishing the relationship between the characteristic band/index and the measurement data, thus improving the accuracy of the SM estimation model. However, the accuracy of SSM estimated only by optical data is poor. By introducing TIR data, the retrieval accuracy of SSM can be improved significantly. It is worth noting that when the optical satellite data are used as the input parameters, the BPNN model is more suitable for the area with flat terrain and gentle slope.

When the quality of RS image varies, it is possible that the spatial distribution of the LST-VI model is unable to form a complete triangle or trapezoid, thus resulting in a significant diference between the estimated SM and the measured value. The model proposed in this study addresses the abovementioned problems while estimating SSM in case of a small sample size. The BPNN model provides a powerful tool for estimating SSM in complex/heterogeneous media (e.g., rough vegetated surfaces). In this paper, the soil moisture retrieved by Landsat-8 and MODIS data has high accuracy. The SSM retrieval model based on the BPNN can be applied to estimate the SSM with diferent spatial resolution.

References

[1] E. A. B. Eltahir, "A soil moisture-rainfall feedback mechanism, 1. Theory and observations," *Water Resources Research*, vol. 34, no. 4, pp. 765–776, 1998.

[2] S. I. Seneviratne, T. Corti, E. L. Davin et al., "Investigating soil moisture-climate interactions in a changing climate: a review," *Earth-Science Reviews*, vol. 99, no. 3-4, pp. 125–161, 2010.

[3] P. Rahimzadeh-Bajgiran, A. A. Berg, C. Champagne, and K. Omasa, "Estimation of soil moisture using optical/thermal infrared remote sensing in the Canadian Prairies," *ISPRS Journal of Photogrammetry and Remote Sensing*, vol. 83, pp. 94–103, 2013.

[4] I. M. Ferguson, J. L. Jeferson, R. M. Maxwell, and S. J. Kollet, "Efects of root water uptake formulation on simulated water and energy budgets at local and basin scales," *Environmental Earth Sciences*, vol. 75, no. 4, p. 316, 2016.

[5] P. Falloon, C. D. Jones, M. Ades, and K. Paul, "Direct soil moisture controls of future global soil carbon changes: an important source of uncertainty," *Global Biogeochemical Cycles*, vol. 25, no. 3, p. 3010, 2011.

[6] W. Dorigo and R. De Jeu, "Satellite soil moisture for advancing our understanding of earth system processes and climate change," *International Journal of Applied Earth Observation and Geoinformation*, vol. 48, pp. 1–4, 2016.

[7] M. Hosseini and M. R. Saradjian, "Soil moisture estimation in a vegetated area using combination of AIRSAR and landsat5-TM images," *Journal of the Indian Society of Remote Sensing*, vol. 42, no. 4, pp. 719–726, 2014.

[8] D. Baldwin, S. Manfreda, H. Lin, and E. A. Smithwick, "Estimating root zone soil moisture across the Eastern United States with passive microwave satellite data and a simple hydrologic model," *Remote Sensing*, vol. 11, no. 17, p. 2013, 2019.

[9] S. Elbialy, A. Mahmoud, B. Pradhan, and M. Buchroithner, "Application of spaceborne synthetic aperture radar data for extraction of soil moisture and its use in hydrological modelling at Gottleuba Catchment, Saxony, Germany," *Journal of Flood Risk Management*, vol. 7, no. 2, pp. 159–175, 2014.

[10] S. Koley and C. Jeganathan, "Estimation and evaluation of high spatial resolution surface soil moisture using multi-sensor multi-resolution approach," *Geoderma*, vol. 378, no. 15, Article ID 114618, 2020.

[11] W. W. Verstraeten, F. Veroustraete, and J. Feyen, "Assessment of evapotranspiration and soil moisture content across diferent scales of observation," *Sensors*, vol. 8, no. 1, pp. 70–117, 2008.

[12] A. A. Hassaballa, O. F. Althuwaynee, and B. Pradhan, "Extraction of soil moisture from RADARSAT-1 and its role in the formation of the 6 december 2008 landslide at bukit antarabangsa, kuala lumpur," *Arabian Journal of Geosciences*, vol. 7, no. 7, pp. 2831–2840, 2014.

[13] A. Tabatabaeenejad, M. Burgin, X. Duan, and M. Moghaddam, "P-band radar retrieval of subsurface soil moisture profifile as a second-order polynomial: fifirst AirMOSS results," *IEEE T Geosci Remote*, vol. 53, no. 2, pp. 645–658, 2015.

[14] M. Sadeghi, S. B. Jones, and W. D. Philpot, "A linear physically-based model for remote sensing of soil moisture using short wave infrared bands," *Remote Sensing of Environment*, vol. 164, pp. 66–76, 2015.

[15] H. H. Nguyen, S. Cho, and M. Choi, "Spatial soil moisture estimation in agro-pastoral transitional zone based on synergistic use of SAR and optical-thermal satellite images," *Agricultural and Forest Meteorology*, vol. 312, no. 7, Article ID 108719, 2022.

[16] A. J. Peters, E. A. Walter-Shea, L. Ji, A. Vina, M. Hayes, and M. D. Svoboda, "Drought monitoring with NDVI-based standardized vegetation index," *Photogrammetric Engineering & Remote Sensing*, vol. 68, no. 1, pp. 71–75, 2002.

[17] A. Ghulam, Q. Qin, and Z. Zhan, "Designing of the perpendicular drought index," *Environmental Geology*, vol. 52, no. 6, pp. 1045–1052, 2007a.

[18] M. Amani, S. Parsian, S. M. MirMazloumi, and O. Aieneh, "Two new soil moisture indices based on the NIR-red triangle space of Landsat-8 data," *International Journal of Applied Earth Observation and Geoinformation*, vol. 50, pp. 176–186, 2016.

[19] R. Nemani, L. Pierce, S. Running, and S. Goward, "Developing satellite-derived estimates of surface moisture status," *Journal of Applied Meteorology*, vol. 32, no. 3, pp. 548–557, 1993.

[20] K. Czajkowski, S. Goward, S. J. Stadler, and A. Walz, "Thermal remote sensing of near surface environmental variables: application over the Oklahoma Mesonet," *The Professional Geographer*, vol. 52, no. 2, pp. 345–357, 2000.

[21] G. P. Petropoulos, G. Ireland, and B. Barrett, "Surface soil moisture retrievals from remote sensing: current status, products & future trends," *Physics and Chemistry of the Earth, Parts A/B/C*, vol. 83-84, pp. 36–56, 2015.

[22] T. N. Carlson, R. R. Gillies, and E. M. Perry, "A method to make use of thermal infrared temperature and NDVI measurements to infer surface soil water content and fractional vegetation cover," *Remote Sensing Reviews*, vol. 9, no. 1-2, pp. 161–173, 1994.

[23] S. Stisen, I. Sandholt, A. Nørgaard, R. Fensholt, and K. H. Jensen, "Combining the triangle method with thermal inertia to estimate regional evapotranspiration: applied to MSG-SEVIRI data in the Senegal River basin," *Remote Sensing of Environment*, vol. 112, no. 3, pp. 1242–1255, 2008.

[24] N. R. Patel, R. Anapashsha, S. Kumar, S. K. Saha, and V. K. Dadhwal, "Assessing potential of MODIS derived temperature/vegetation condition index (TVDI) to infer soil moisture status," *International Journal of Remote Sensing*, vol. 30, no. 1, pp. 23–39, 2009.

[25] W. Wang, D. Huang, X. G. Wang, Y. R. Liu, and F. Zhou, "Estimation of soil moisture using trapezoidal relationship between remotely sensed land surface temperature and vegetation index," *Hydrology and Earth System Sciences*, vol. 15, no. 5, pp. 1699–1712, 2011.

[26] H. Sun, "Two-stage trapezoid: a new interpretation of the land surface temperature and fractional vegetation coverage space," *Ieee Journal of Selected Topics in Applied Earth Observations and Remote Sensing*, vol. 9, no. 1, pp. 336–346, 2016.

[27] T. N. Carlson, E. M. Perry, and T. J. Schmugge, "Remote estimation of soil moisture availability and fractional

vegetation cover for agricultural fields," *Agricultural and Forest Meteorology*, vol. 52, no. 1-2, pp. 45–69, 1990.

[28] I. Sandholt, K. Rasmussen, and J. Andersen, "A simple interpretation of the surface temperature/vegetation index space for assessment of surface moisture status," *Remote Sensing of Environment*, vol. 79, no. 2–3, pp. 213–224, 2002.

[29] Z. Wan, P. Wang, and X. Li, "Using MODIS land surface temperature and normalized diference vegetation Index products for monitoring drought in the southern Great Plains, USA," *International Journal of Remote Sensing*, vol. 25, no. 1, pp. 61–72, 2004.

[30] A. Ghulam, Z. L. Li, Q. Qin et al., "A method for canopy water content estimation for highly vegetated surfaces-shortwave infrared perpendicular water stress index," *Science in China, Series A D*, vol. 50, no. 9, pp. 1359–1368, 2007.

[31] M. E. Holzman, R. Rivas, and M. C. Piccolo, "Estimating soil moisture and the relationship with crop yield using surface temperature and vegetation index," *International Journal of Applied Earth Observation and Geoinformation*, vol. 28, pp. 181–192, 2014.

[32] Q. Yuan, H. Xu, T. Li, H. Shen, and L. Zhang, "Estimating surface soil moisture from satellite observations using a generalized regression neural network trained on sparse ground-based measurements in the continental U.S," *Journal of Hydrology*, vol. 580, Article ID 124351, 2020.

[33] A. Elshorbagy and K. Parasuraman, "On the relevance of using artificial neural networks for estimating soil moisture content," *Journal of Hydrology*, vol. 362, no. 1-2, pp. 1–18, 2008.

[34] S. S. Zanetti, R. A. Cecilio, E. G. Alves, V. H. Silva, and E. F. Sousa, "Estimation of the moisture content of tropical soils using colour images and artificial neural networks," *Catena*, vol. 135, pp. 100–106, 2015.

[35] E. Santi, S. Paloscia, S. Pettinato, and G. Fontanelli, "Application of artificial neural networks for the soil moisture retrieval from active and passive microwave spaceborne sensors," *International Journal of Applied Earth Observation and Geoinformation*, vol. 48, pp. 61–73, 2016.

[36] J. Kolassa, R. H. Reichle, Q. Liu et al., "Estimating surface soil moisture from SMAP observations using a Neural Network technique," *Remote Sensing of Environment*, vol. 204, pp. 43–59, 2018.

[37] L. Gao, Q. Gao, H. Zhang et al., "A deep neural network based SMAP soil moisture product," *Remote Sensing of Environment*, vol. 277, Article ID 113059, 2022.

[38] J. Liu, Y. Xu, H. Li, and J. Guo, "Soil moisture retrieval in farmland areas with Sentinel multi-source data based on regression convolutional neural networks," *Sensors*, vol. 21, no. 3, p. 877, 2021.

[39] S. Nativel, E. Ayari, N. Rodriguez-Fernandez et al., "Hybrid methodology using sentinel-1/sentinel-2 for soil moisture estimation," *Remote Sensing*, vol. 14, no. 10, p. 2434, 2022.

[40] X. Yang, C. Zhang, Z. Cui, Y. Fan, and J. Wang, "Yingjuan Han (2018) Filling method for soil moisture based on BP neural network," *Journal of Applied Remote Sensing*, vol. 4, Article ID 42806, 2018.

[41] K. Yang, J. Qin, L. Zhao et al., "A multiscale soil moisture and freeze–thaw monitoring network on the Third Pole," *Bulletin of the American Meteorological Society*, vol. 94, no. 12, pp. 1907–1916, 2013.

[42] R. Zhuang, Y. Zeng, S. Manfreda, and Z. Su, "Quantifying long-term land surface and root zone soil moisture over Tibetan plateau," *Remote Sensing*, vol. 12, no. 3, p. 509, 2020.

[43] M. Sadeghi, E. Babaeian, M. Tuller, and S. B. Jones, "The optical trapezoid model: a novel approach to remote sensing of soil moisture applied to Sentinel-2 and Landsat-8 observations," *Remote Sensing of Environment*, vol. 198, pp. 52–68, 2017.

[44] L. Zhang, Y. Zeng, R. Zhuang et al., "In situ observation-constrained global surface soil moisture using random forest model," *Remote Sensing*, vol. 13, no. 23, p. 4893, 2021.